

Influence of Boron on Austenite to Ferrite Transformation Behavior of Low Carbon Steel Under Continuous Cooling

Soumyajit Koley, Arnab Karani, Soumya Chatterjee, and Mahadev Shome

(Submitted August 9, 2017; in revised form May 10, 2018; published online June 22, 2018)

In the current work, the influence of boron on austenite to ferrite transformation behavior under continuous cooling condition and its associated features, e.g., final microstructure, mechanical properties, etc., in low carbon steel has been studied. The steels (C 0.04 wt.%, B 10–100 ppm) prepared in an open air laboratory furnace showed identical microstructures having ferrite grains of 20–25 μm . However, tensile test data indicate variation of yield strength and ultimate tensile strength with boron content. The yield point elongation and strain aging index both were found to decrease with increase in boron content or boron-to-nitrogen ratio. As the boron nitride precipitates stimulate the nucleation of ferrite phase, the dilation curves show an increase in austenite to ferrite transformation start temperature with boron content. The resulting microstructure and hardness value also corroborate the finding. Transmission electron microscopy findings revealed the presence of ultra-fine boron nitride (BN) precipitates in both grain boundary and grain body of the steel having boron concentration of 30 ppm and beyond. The presence of these precipitates also increased with boron content. Based on austenite decomposition behavior, related microstructure and hardness values it is conjectured that these BN precipitates may act as nucleating agent for polygonal ferrite during austenite decomposition, thereby softening the steel during fast cooling.

Keywords BN precipitate, boron-treated steel, continuous cooling transformation (CCT) diagram, transmission electron microscopy

1. Introduction

Boron is a unique alloy addition to steel which increases the hardenability of steel up to a critical concentration (Ref 1–3). Beyond this concentration, it decreases the hardenability of the steel. The primary effect of boron on the steel hardenability is to raise the energy barrier to ferrite nucleation at the austenite grain boundaries (Ref 4). Although the mechanisms involved are not yet fully understood, free boron is known to segregate extensively to the austenite grain boundaries where it reduces the grain boundary energy (Ref 5–7). Based on the transformation kinetics theory, it can be rationalized that a decrease in the austenite grain boundary energy will suppress the nucleation of the ferrite at these sites (Ref 8). As a result, either the austenite would retain up to sufficiently lower temperature or it may transform to martensite or bainite (depending on the chemistry and cooling rate) instead of transforming to ferrite (Ref 9). Once the austenite transforms to harder phase(s) like martensite or bainite instead of soft ferrite, it is obvious that the strength and hardness of the steel will increase. However, it should be noted that the effectiveness of boron as a harden-

ability element is a contingent upon an effective protection of boron from nitrogen and oxygen through sufficient additions of titanium and aluminum.

Melloy (Ref 1) and Taylor et al. (Ref 10) had reported an optimum boron range for maximum hardenability in 0.2%-C steel was 15–25 ppm. Further addition of boron deteriorates the hardenability of the steel by promoting formation of polygonal ferrites (Ref 1, 11, 12). The reason behind this is primarily considered to be precipitation of the “boron constituents” on the prior austenite grain boundaries which can act as the preferential nucleation sites for austenite to ferrite transformation (Ref 13, 14). However, the phase(s) which act(s) as the “boron constituents” is a matter of ambiguity. Earlier researchers like Ohmori et al. (Ref 15), Maitrepierre et al. (Ref 16) and Melloy (Ref 1) worked on the effect of boron on low alloy mild steel containing 0.15–0.25% carbon and concluded that the precipitation of complex boro-carbide, like $M_{23}(BC)_6$, acts as the preferential nucleation sites for ferrite. However, the works of Simcoe et al. (Ref 13) and Sharma et al. (Ref 17) indicate that this kind of complex boro-carbides may enhance the energy barrier to ferrite nucleation due to an increase in the total strain energy of the embryo at the grain boundary. In addition, these precipitates have been proposed to inhibit ferrite nucleation at the early stages of transformation owing to their semi-coherent nature. The inhibition of ferrite nucleation at the coherent side of the austenite grain boundary has been verified experimentally (Ref 18).

Parusov et al. (Ref 19) had indicated that the precipitation of BN on the grain boundary might be responsible for favoring ferrite formation. Improvement of ductility, workability and impact toughness of such steel due to the presence of ferritic microstructure has been confirmed by other researchers also (Ref 20, 21). Anjana Deva et al. (Ref 22) had shown that the ferrite grain size of steel with boron was coarser as compared to that in the case of boron free steel. The reason for coarse ferrite

Soumyajit Koley, Arnab Karani, Soumya Chatterjee, and Mahadev Shome, Research and Development, Tata Steel, Jamshedpur, Jharkhand 831 001, India. Contact e-mails: soumyajitkoley@gmail.com, s.koley@tatasteel.com.

grains in boron-containing steel was attributed to the presence of coarse boron nitride (BN) precipitates as nucleating site instead of fine aluminum nitride (AlN) in steel without boron. Larger ferrite grain size in boron-added steel was also reported in the work of Kim, which they referred to the precipitation of BN as well as higher density of cementite (Ref 23). Similarly, Camurri et al. (Ref 24) had proposed an alternative mechanism of lowering of strength and hardness of the steel by the precipitation of boron nitrides (BN) taking place with appreciably higher boron content. This scavenging action decreases the nitrogen content in solid solution and obviously attenuating the hardening effect due to the presence of interstitial elements. As a consequence, the yield stress decreases and the ductility increases.

All these former work were primarily carried out with mild steel having 0.1-0.25 wt.% carbon along with boron content within 30 ppm. There are very limited numbers of literatures where effect of boron has been studied on steels having carbon content less than 0.1 wt.% (Ref 22, 25). However, to the authors' best belief and knowledge there is hardly any data available in the public domain on effect of addition boron more than 50 ppm in steel containing 0.03-0.05% carbon. In the present work, authors tried to investigate the effect of boron addition (in the range of 10-100 ppm) on the austenite to ferrite transformation behavior under continuous cooling condition of low carbon steel (0.04%). Also the influence of boron content on the final microstructure and properties of the steel have been studied.

2. Experimental

2.1 Laboratory Heat Making

Low carbon, low silicon, aluminum-killed steels with variable boron content (10-100 ppm) were made experimentally in an open air induction furnace (25 kg). The chemical composition of the steels was determined by optical emission spectroscopy (OES) and listed in Table 1. At least 3 measurements were done, and the arithmetic mean of those data is presented in Table 1. No special treatment was given to reduce or control the nitrogen content of the steel. The liquid steel was poured in a pre-heated steel mold (cross section 100 × 100 mm) by top-pouring method. After solidification and cooling to room temperature, the hot top was cutoff. In order to homogenize the chemical composition and to break the cast microstructure, the ingots were hot-forged at 1523 K (1250 °C) with an open die forging hammer. The final cross section of the forged bars was 50 × 50 mm. Samples required for further investigations were machined from these forged bars.

Table 1 Chemical composition of the experimentally made steels

Heat no.	C, wt.%	Mn, wt.%	Si, wt.%	S, wt.%	P, wt.%	B, ppm	N, ppm
01	0.045	0.078	0.019	0.007	0.007	10	30
02	0.055	0.096	0.033	0.007	0.008	30	49
03	0.05	0.08	0.02	0.006	0.008	70	77
04	0.04	0.09	0.014	0.008	0.009	100	46

2.2 Tensile Testing

Tensile properties were evaluated employing Instron 5582 universal testing machine at a cross-head velocity of 5 mm/min with 25 mm gauge length, resulting in a nominal strain rate of $3.34E-3 \text{ s}^{-1}$. Cylindrical tensile samples were fabricated, keeping the tensile axis parallel to the direction of maximum dimension of the forged bars. Apart from measuring yield stress (YS), ultimate tensile strength (UTS) and percentage elongation (%El), the yield point elongation (YPE) was also determined from the stress-strain data as per the ASTM E8 standard. The fracture surfaces generated in the tensile test were observed using secondary electrons in a scanning electron microscope (SEM) to determine possible failure mode.

2.3 Strain Aging Index (SAI)

Measurement of strain aging index (SAI) was carried out using the same cylindrical samples used for tensile testing. The specimen were pre-strained in tension by 10% at room temperature, then aged and restrained to failure. The percentage increase in flow stress as a result of restraining was taken as SAI. The aging treatment consisted of 60 min holding at 373 K (100 °C), carried out in boiling water, which is considered to be equivalent to approximately 6 weeks of natural aging at room temperature (Ref 26).

2.4 Microstructural Observation

Specimens for optical microscopy were prepared by conventional grinding and polishing techniques. Polished specimens were etched for 20 s in 4% picral solutions followed by 15 s in 2% nital solutions to reveal the microstructure. The etched samples were observed under a Leica DM6000M optical microscope.

Samples cooled slowly in still air from 1523 K (1250 °C) were used for examining under the transmission electron microscope (TEM). Specimens were prepared by thinning down the steel samples to less than 100 μm thickness followed by punching out a 3-mm disk and further thinning down to electronic transparent range by twin jet electro-polishing. The prepared samples were observed under a Phillips CM 200 transmission electron microscope (TEM). Images were captured using both bright-field (BF) and dark-field (DF) modes and obtained with the microscope operating at 200 kV of accelerating voltage. Selected area electron diffraction (SAED) patterns of the desired areas (precipitates, grain boundaries, etc.) were recorded and subsequently indexed using the ratio method.

2.5 Dilatometric Study

Dilatometric studies were performed in a Gleeble 1500D thermo-mechanical simulator. The samples were of 6 mm

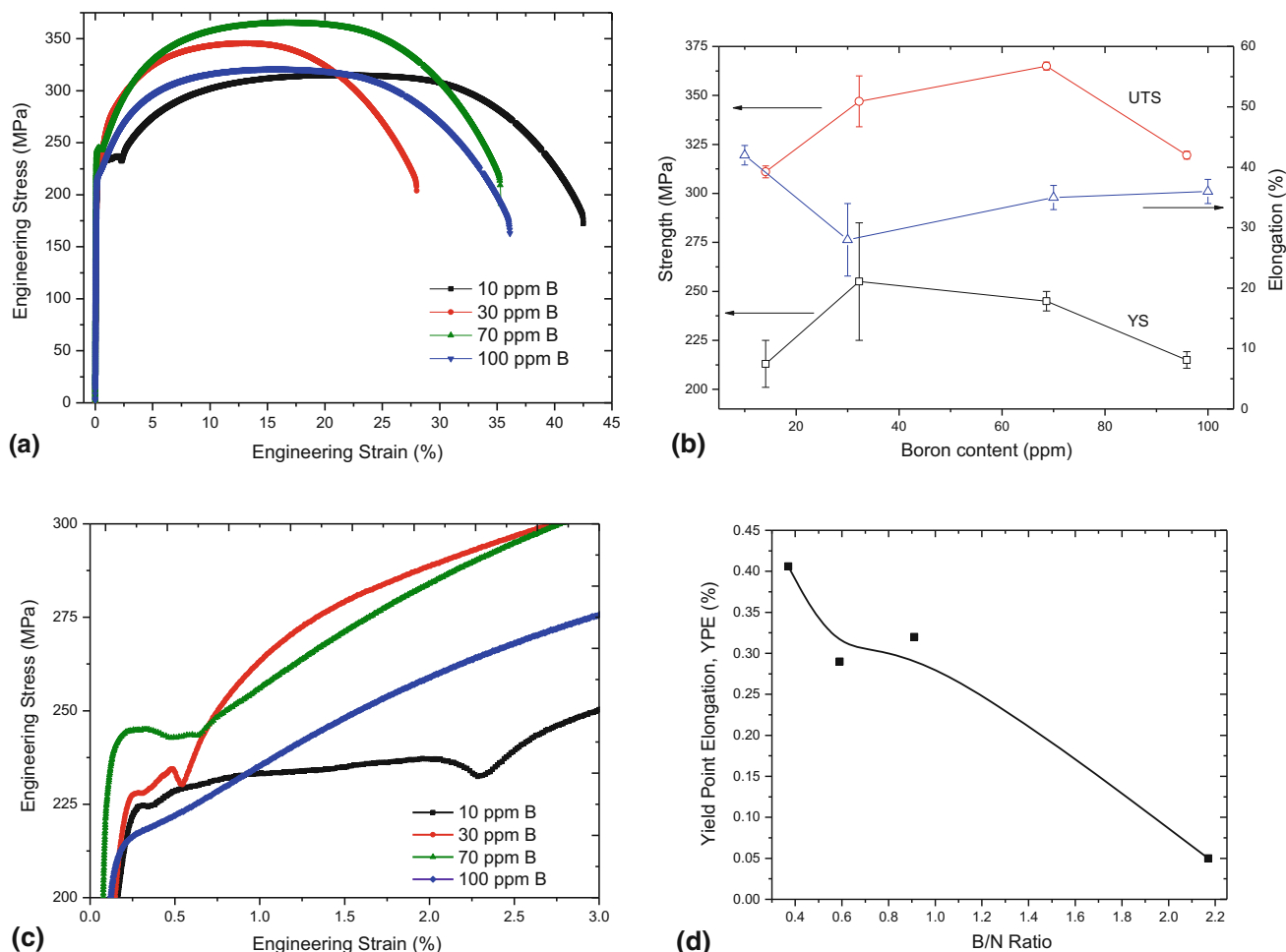


Fig. 1 (a) Engineering stress vs. engineering strain plots for all four steels. (b) Variation of YS, UTS and %El with boron content of the experimental steels. (c) Magnified view of Fig. 1(a), showing yield point elongation. (d) Variation of yield point elongation as a function of boron-to-nitrogen ratio of the steels

diameter and 90 mm length machined from forged bars. A platinum–platinum–rhodium thermocouple was upset-butt-welded on the surfaces of the samples for monitoring and controlling the temperature through a closed circuit feedback control loop. The samples were heated at 5 K/s up to 1273 K (1000 °C), held there for 300 s and subsequently cooled to room temperature under different cooling rates in the range of 0.1–75 K/s. Prior to heating the Gleeble chamber was evacuated and refilled with high-purity argon gas at low pressure to protect the steel samples from oxidation. The dilatometer attached diametrically on the central hot zone of the sample recorded the dilatation behavior as a function of time and temperature.

3. Results

3.1 Physical and Mechanical Properties

Figure 1(a) depicts the engineering stress–strain curves corresponding to the steels having boron content varying in the range of 10–100 ppm. The YS, UTS and percentage elongation (%El) values were plotted separately as a function of boron content in Fig. 1(b). Both the YS and UTS show a broad

crest corresponding to the steels having 30–70 ppm boron. As the boron content increases to 100 ppm, both these parameters decrease notably resulting in softer steel. A similar observation was reported by Melloy et al. for molybdenum- and titanium-added steels having 0.1–0.2 wt.% carbon (Ref 1). However, in that case, the increase in YS as a function of boron content resulted in distinctly sharp maxima instead of a broad hump observed in this investigation. This anomaly may be attributed to the differences in steel chemical compositions. The work of Deva et al. (Ref 22) demonstrates that addition of boron in low carbon steel favors coarsening of the dislocation cell size under strained condition which actually favors lowering of strength. Figure 2(a–d) depicts that there is hardly any difference in the ferrite grain size for the microstructure of the as-forged steels. Hence, coarsening of dislocation cell might be one of the reasons for obtaining the lowest strength for steel having 100 ppm boron. The ductility in terms of percentage elongation (%El) when plotted against boron content depicts a sudden drop when boron increases from 10 to 30 ppm; however, beyond 30 ppm it remains constant for all other steels.

Serrated yielding behavior of the steels was evident from Fig. 1(c), which is a magnified view of the engineering stress–strain plot focussing on the yield onset region. The YPE values are plotted with boron-to-nitrogen ratio in Fig. 1(d). A

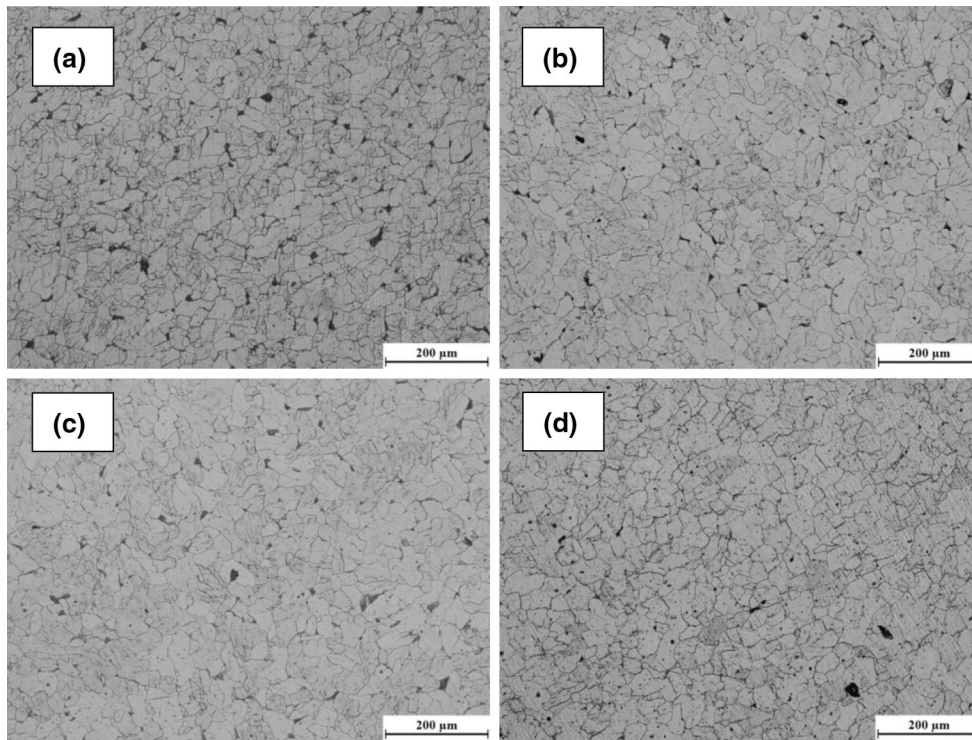


Fig. 2 Optical micrographs of the as-forged steels having (a) 10, (b) 30, (c) 70 and (d) 100 ppm boron

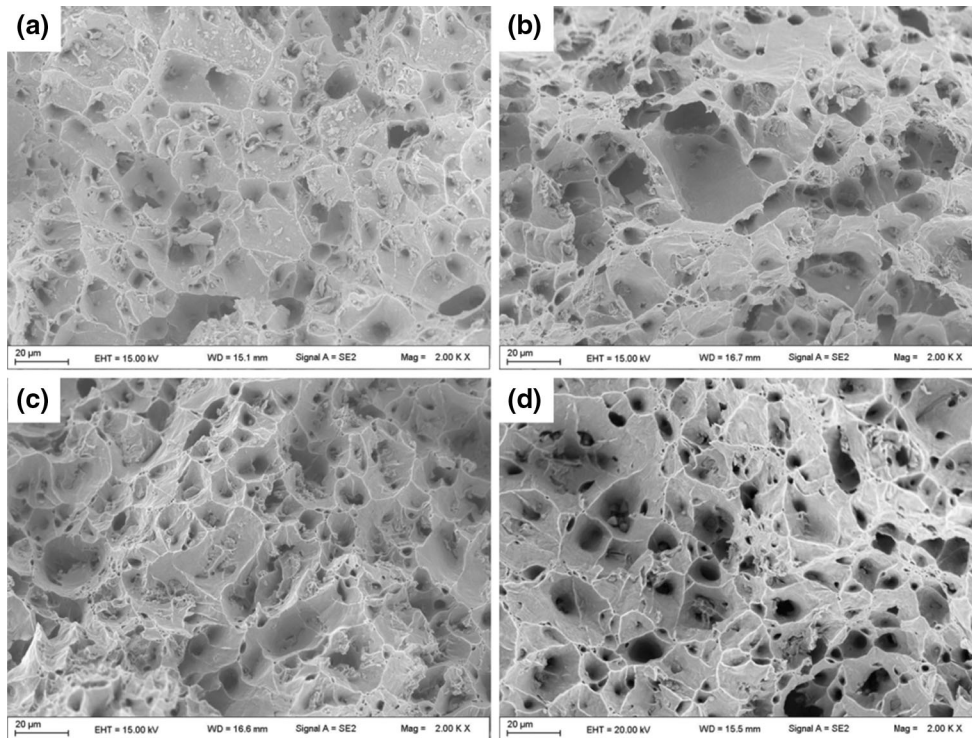


Fig. 3 Scanning electron fractographs of the fracture surfaces of the tensile-tested specimens of the steels containing (a) 10, (b) 30, (c) 70 and (d) 100 ppm boron

conspicuous decrease in the YPE value from 0.4 to 0.05 with increase in the ratio from 0.37 to 2.17 can be observed.

The occurrence of serrated yielding is universally attributed to the presence of free carbon and nitrogen in the iron lattice

which sequentially locks and unlocks the dislocations during the straining process.

Figure 3(a-d) represents photomicrographs of the fracture surface obtained during the quasi-static tensile test of the steel

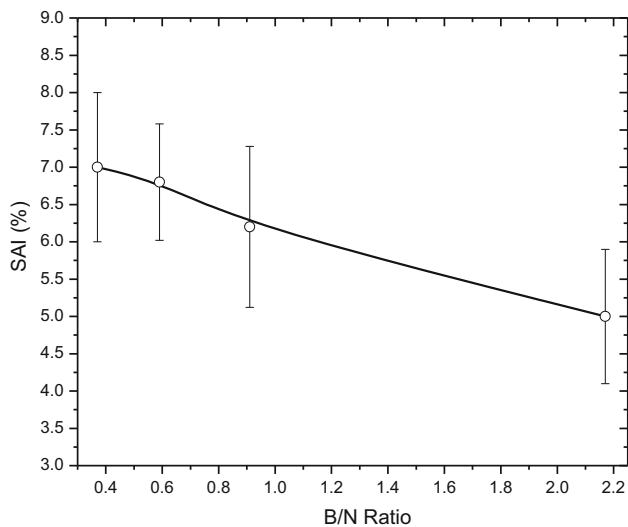


Fig. 4 Variation of strain aging index (SAI) as function of the boron-to-nitrogen ratio of steels

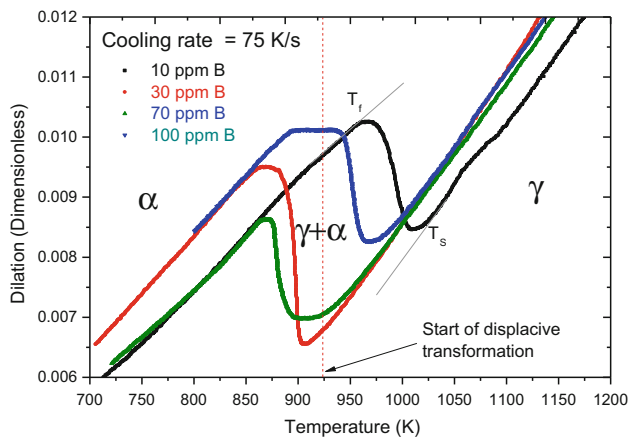


Fig. 5 Dilation curves of four different steels recorded while cooling the samples from 1273 K (1000 °C) at 75 K/s

specimens containing 10-100 ppm of boron. In all four images, conspicuous presence of equiaxial dimples can be observed which supports ductile failure of the materials. Apart from this, it should also be noted that the qualitative analyses of fractographs display relatively less amount of dimples for specimens containing lower amount of boron (such as 10 and 30 ppm) compared to specimens having higher amount of boron (70 and 100 ppm). Fine boron nitride (BN) precipitates might have acted as the accumulation point of micro-voids which under increasing tensile load grew in size and finally coalesce with each other to form the primary fracture surface. Specimens having higher boron led to precipitation of higher amount of BN and thus higher numbers of dimples in the fracture surface.

The SAI value measured for all four steels is plotted as a function of boron-to-nitrogen ratio in Fig. 4. A gradual but definite decrease in the SAI value could be noticed with increase in the boron-to-nitrogen ratio from 0.37 to 2.17. Steel containing 100 ppm boron (boron-to-nitrogen ratio 2.17) shows that the SAI value of 5 which indicates the steel to be very less susceptible to strain aging (Ref 26). The cause for strain aging

is the presence of interstitial solute atoms like carbon and nitrogen in iron lattice (Ref 27). According to Cottrell and Bilby, the mechanism of strain aging is the pinning of moving dislocations by these solute atoms (Ref 28). It has been reported by Baird (Ref 29) and Wilson et al. (Ref 30) that for annealed steel the presence of even 1 ppm of interstitial solute is sufficient to cause detectable strain aging and 5-10 ppm of solute may cause severe strain aging. In the current work, the result showed that the steels showed negligible YPE and SAI value less than 6 despite containing high amount of the solute nitrogen (30-80 ppm). Interestingly, this makes the steel immune to strain aging process. This is only possible since the boron-to-nitrogen ratio attains an appreciably high value of 2.17 for the steel having 100 ppm boron. Boron has strong affinity toward nitrogen and carbon, and it forms nitride and carbide/boro-carbide while the cooling occurs from liquid phase during the casting process (Ref 31, 32). The microstructure which forms is thus free from any interstitial solute atoms such as carbon and nitrogen. This eventually results in both smooth yielding and low strain aging. Thus, boron-to-nitrogen (or B/N) ratios higher than 2 would lead to a steel suitable for applications where smooth yielding behavior and reduced strain aging effect is necessary.

3.2 Continuous Cooling Transformation Diagram

Figure 5 shows the dilation curves recorded for steels containing 10, 30, 70 and 100 ppm boron while cooling at a rate of 75 K/s. Dilation plots corresponding to only one cooling rate are shown for representation purpose. Linear portion of the plots, observed either below 848 K (575 °C) or above 1023 K (750 °C), represents dilation originating from a single phase possibly either the ferrite (α) at lower temperature or the austenite (γ) at higher temperature. Between 848 K (575 °C) and 1023 K (750 °C), there is a clear change in slope for plots corresponding to all four steels. This occurs due to the austenite to ferrite phase transformation. Two important points of inflection viz. T_s and T_f are indicated in this figure. They represent the start and finish temperatures of the austenite to ferrite transformation.

One observation could be made out from these plots that within the temperature range where the phase transformation is taking place, the plots showed a single slope, possibly indicating that only one phase transformation was taking place in that temperature range.

The temperature and time corresponding to transformation start (T_s and t_s) and transformation finish (T_f and t_f) of austenite to ferrite were noted from dilation curves corresponding to four steels subjected to different cooling rates in the range of 0.1–75 K/s. Plotting of these time–temperature data for all the cooling rates produced the CCT diagrams for the steels used for the experiments (Fig. 6a-d).

From the CCT diagrams (Fig. 6a-d), few observations could be made. First, all the four diagrams are distinctly showing three zones, from high to low temperature, corresponding to austenite (γ), dual-phase field and ferrite (α) phases. Second, lines joining T_s and T_f of the steels containing 10, 30 and 70 ppm boron have shifted marginally toward lower time compare to that of steel having 100 ppm boron. This indicates that a lower critical cooling rate exists for higher boron content. Third, in all the four steels, the T_f was found to vary in the range of 1073 K (800 °C) to 823 K (550 °C). Hence, it is more

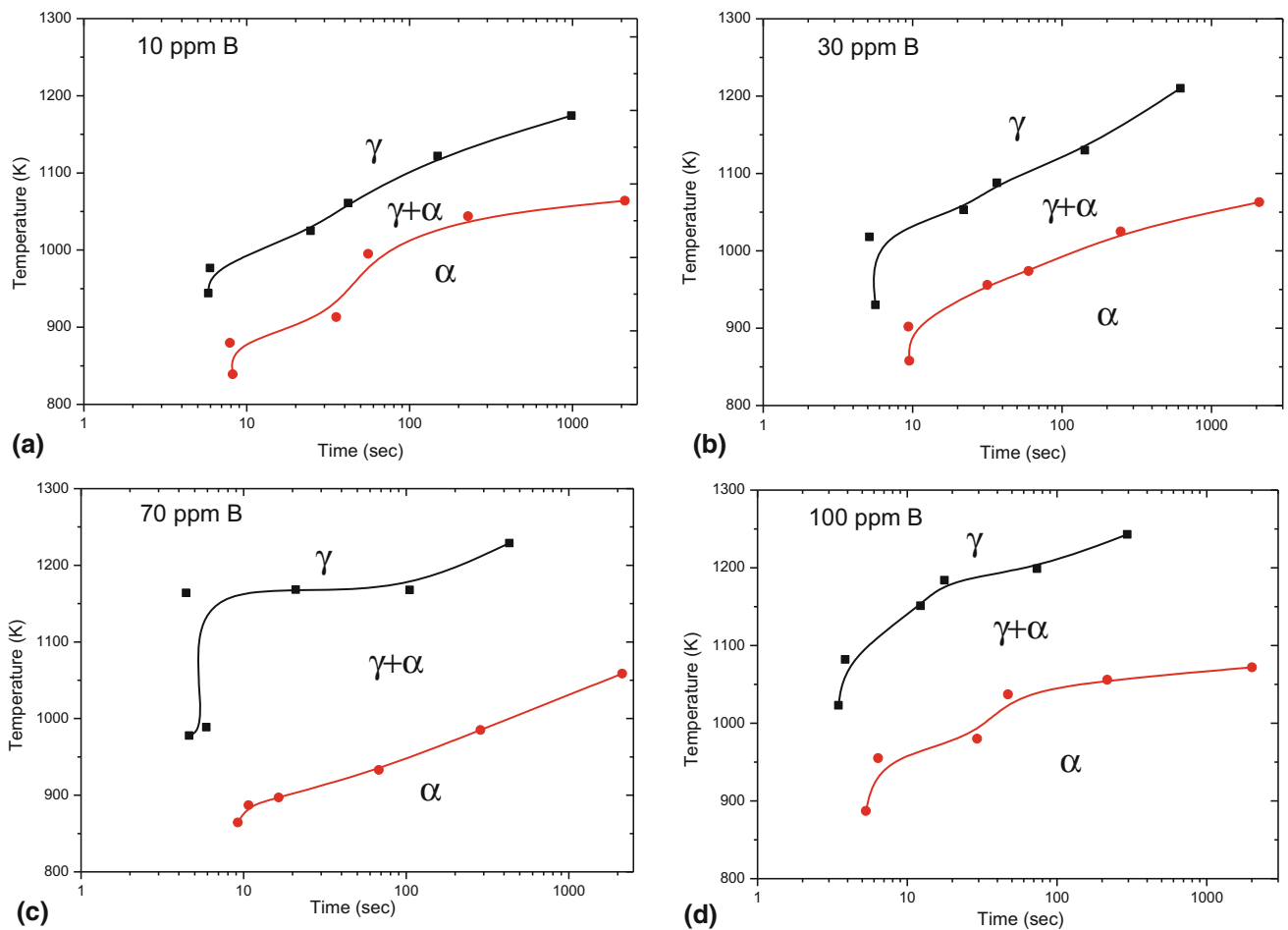


Fig. 6 CCT diagrams constructed from dilation curves for steels containing (a) 10, (b) 30, (c) 70 and (d) 100 ppm boron

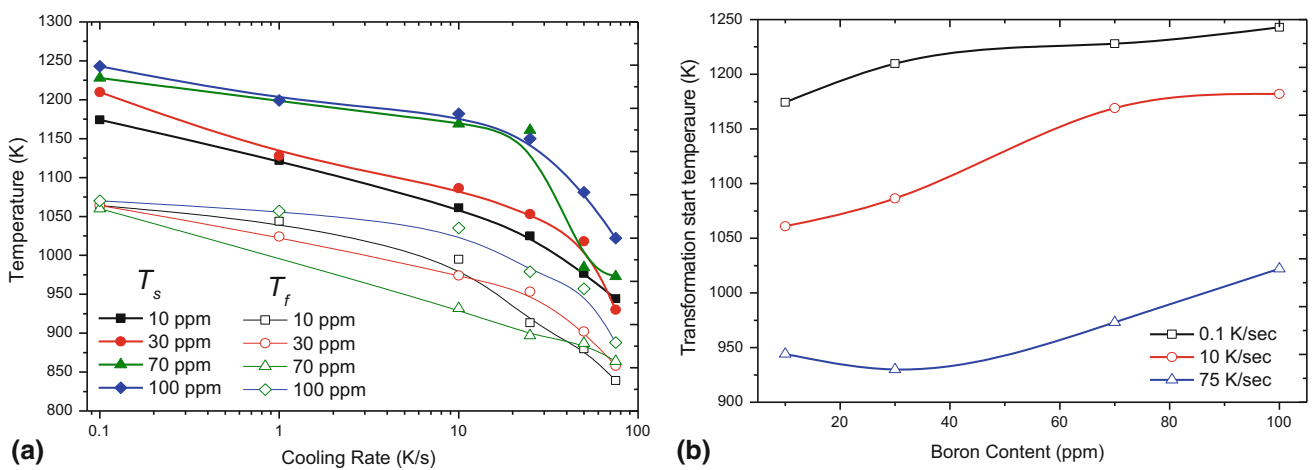


Fig. 7 (a) Temperatures corresponding to austenite to ferrite transformation start (T_s) and transformation finish (T_f) are plotted as function of cooling rate for steel samples having variable boron content. (b) Temperature corresponding to austenite to ferrite transformation start (T_s) is plotted as function of boron content of the steel for different cooling rates 0.1, 10 and 75 K/s

likely to produce the polygonal ferrite for the higher T_f as the dominating phase(s) in the microstructure.

In Fig. 7(a), the temperature corresponding to transformation start (T_s) and transformation finish (T_f) were plotted as a function of cooling rates. It is observed that both the temperatures decrease gradually as the cooling rate increases

from 0.1 to 25 K/s; however, cooling rates higher than 25 K/s reduce the transformation temperatures (both T_s and T_f) more effectively.

Figure 7(b) describes the variation of T_s with boron content in the steel for three different cooling rates. A conspicuous increase of T_s is observed as boron content in the steel

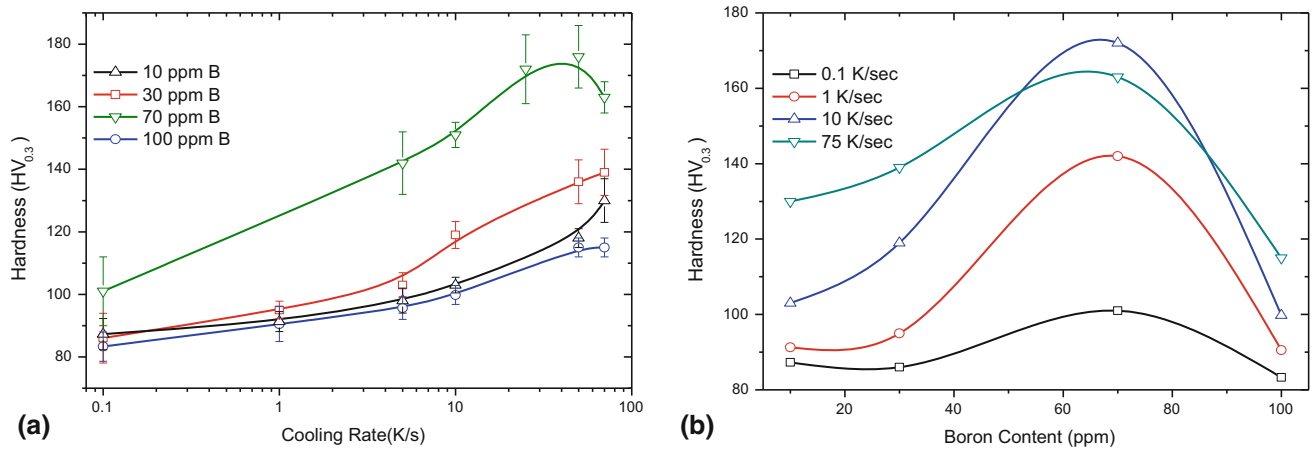


Fig. 8 Variation of hardness plotted with (a) cooling rate and (b) boron content for the steels samples used in the dilatometry

increases. Even for a very slow cooling rate of 0.1 K/s, an increment of temperature by ~ 70 K could be noticed for increase in boron content from 10 to 100 ppm.

The hardness measured on the polished cross section of the samples used for dilatometry is plotted as a function of cooling rate and boron content of the steel in Fig. 8(a) and (b). A monotonic increase in the hardness with the cooling rate is observed for samples having 10, 30 and 100 ppm boron (Fig. 8a). A noticeable finding was the sample with 100 and 70 ppm boron showing the minimum and the maximum hardness for the different cooling rates, respectively. In Fig. 8(b), the hardness is the maximum in sample having 70 ppm boron. Similar trend had been shown by researcher(s) earlier; however, the peak hardness there was corresponding to 15-30 ppm boron instead of 70 ppm boron in the present investigation (Ref 1). This discrepancy might be owing to difference in the overall steel chemistry, as showed by Maitrepierre et al. (Ref 16).

In Fig. 9, optical micrographs of the four steels subjected to holding at 1273 K (1000 °C), followed by cooling at rates in the range of 0.1-75 K/s, are tabulated. All the slowly cooled samples, i.e., 0.1 and 1 K/s show coarse-grained ferritic microstructure with occasional presence of small pearlite colonies, independent of the steel chemistry. However, samples cooled at moderate cooling rate (10 K/s) show different microstructures depending on the boron content. Samples having 10 and 100 ppm boron are showing irregular-shaped and coarse-grained quasi-polygonal ferrite. Quasi-polygonal ferrite is similar to polygonal ferrite; however, it possesses irregular grain boundary unlike polygonal ferrite owing to its lower transformation temperature (Ref 33, 34). The grain morphology of quasi-polygonal ferrite formed at medium cooling rate is relatively more irregular than that of ferrite formed at low cooling rate in low carbon steels (Ref 35). Microstructures obtained for the samples having 30 and 70 ppm boron show the presence of the quasi-polygonal ferrite with higher degree of irregularity. The former sample also shows ferrite with predominance of microstructure with acicular shape. As the cooling rate increases to 50 and 75 K/s, the variation in microstructure with boron content becomes more conspicuous. In these cooling rates, samples having 100 ppm boron show maximum amount of polygonal ferrite in the microstructure. The three other samples show a microstructure containing substantial amount of acicular ferrite along with

quasi-polygonal ferrite and some Widmanstatten ferrite. In general, the acicularity in the microstructure for these three samples (i.e., samples with 10, 30 and 70 ppm boron) is substantially higher as compared to that of the sample having 100 ppm boron, when cooled at higher rate. However, it could be observed that at higher cooling rates the microstructure becomes finer for all the samples irrespective of boron content.

One important observation is that the volume fraction of phase(s) other than the polygonal ferrite such as pearlite is miniscule and lower than the detection limit of dilatometer used in the study. Hence, dilation curves as well as the CCT diagrams failed to describe clear bays for those phase(s).

These microstructural findings corroborate well with the data obtained for hardness values measured on the same samples. As the microstructure of the steel having 100 ppm boron shows the maximum fraction of a polygonal ferrite, it is expected to have the least hardness. Meanwhile, for other samples which show substantial degree of acicularity in the microstructure, is accompanied by higher hardness. Hardness data shown in Fig. 8(a) and (b) re-established these facts.

3.3 Characterization of the Precipitates

Dark-field images of the ferrite grain boundaries (Fig. 10a, c, and e) and the corresponding SAED patterns (Fig. 10b, d, f) are listed in Fig. 10. For the sample having 10 ppm boron, a clean grain boundary was observed (Fig. 10a) at sufficiently high magnification. Even a SAED pattern (Fig. 10b) recorded from the same region (marked with a white box in Fig. 10a) revealed the presence of the ferrite phase. Most of the specimens showed clean grain boundaries devoid of any precipitates. However, the scenario was different for the samples having higher boron contents. Figure 10(c) and (e) shows photomicrographs of the ferrite grain boundaries of steels having 30 and 100 ppm boron, respectively. In both these figures, the grain boundaries were found to be decorated with precipitates of nanometric dimension. It can also be noticed—by qualitative analyses of TEM images—that the area fraction of the precipitates increases as boron content increases from 30 to 100 ppm. SAED patterns recorded from precipitates of 30 and 100 ppm boron steel (Fig. 10d, f, respectively) clearly indicate appearance of faint spots along with the bright spots which are originating from the diffraction of electron beam

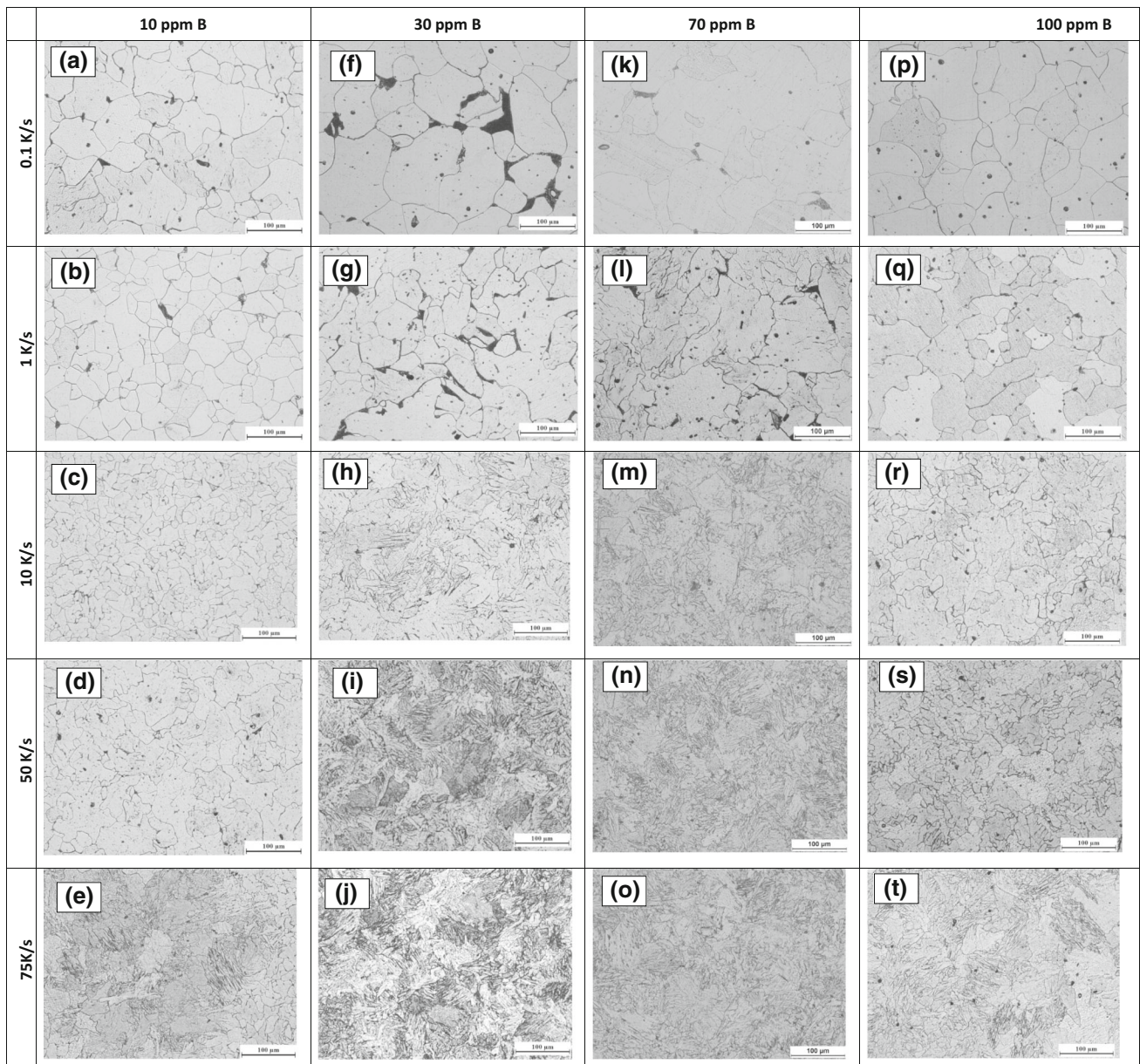


Fig. 9 Optical micrographs of the samples having variable boron content and cooled at different cooling rates

through the matrix. Indexing of patterns consisting of faint spots was carried out followed by calculation of the lattice parameters. Comparing the calculated lattice parameters with the standard value confirmed that the faint spots have originated from face centered cubic (FCC) crystal structure of boron nitride (BN) precipitates. A representative selected area electron diffraction (SAED) pattern of such precipitates with the planar indices h , k and l is given in Fig. 11. Miller indices marked with red boxes are of the faint spots occurring owing to electron beam diffraction through BN precipitates.

4. Discussions

There are three interesting observations from the dilation curves obtained for the four steel samples under different cooling rates. They are as follows:

1. The transformation start temperature (T_s) increased monotonically (irrespective of the cooling rate) with boron content in the steel (Fig. 7b). For fast cooling (75 K/s), T_s increased from 948 K (675 °C) to 1023 K (750 °C) and for slow cooling (0.1 K/s) from 1173 K (900 °C) to 1248 K (975 °C), respectively, with increase in boron content from 10 to 100 ppm. Higher austenite decomposition temperature supports the formation of polygonal ferrite of lower hardness. Higher volume fraction of boron nitride precipitates in the steel containing 100 ppm boron helped in early formation of polygonal ferrite by acting as nucleation sites.
2. The steels having 30 and 70 ppm boron showed that the onset of austenite to ferrite transformation is around 973 K (700 °C) (Fig. 5). However, majority of the reaction takes place below 923 K (650 °C) which is the temperature corresponding to the start of displacive transformation (austenite to acicular ferrite or bainite) cal-

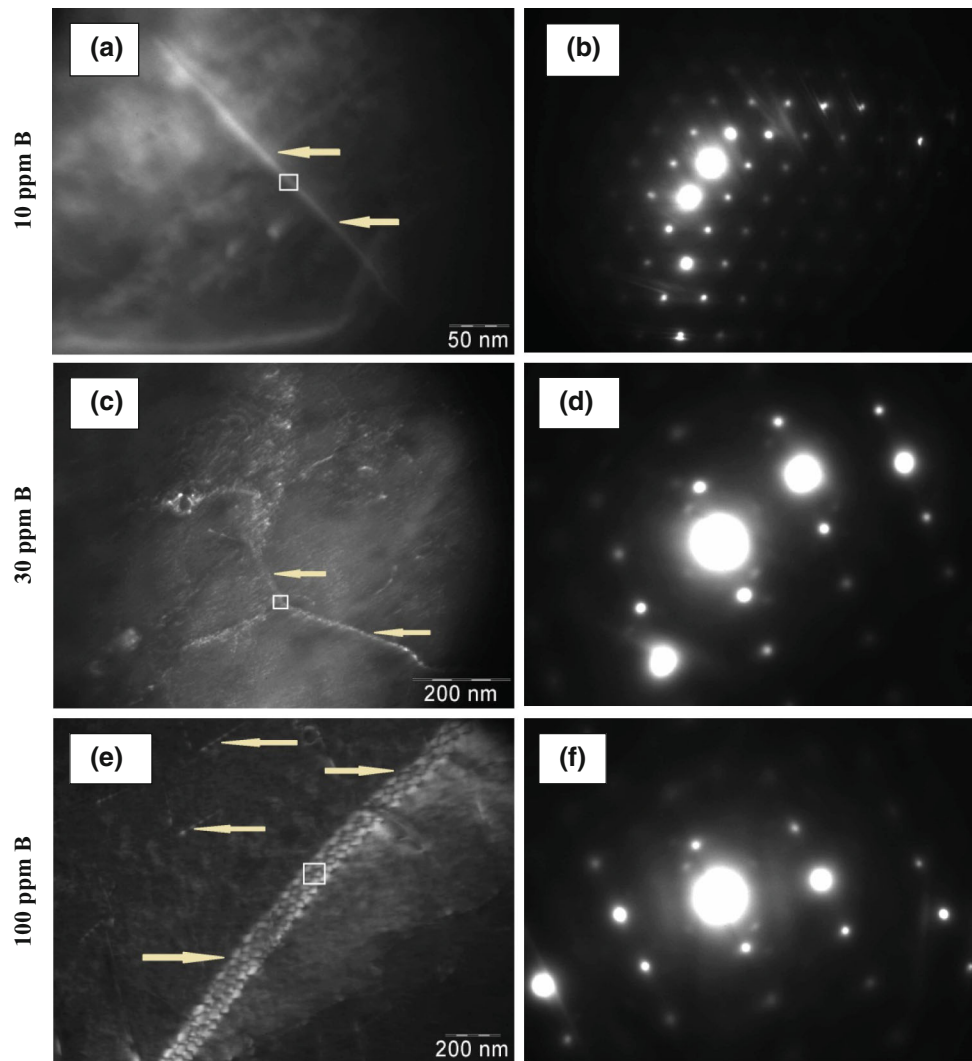


Fig. 10 Dark-field images [(a), (c) and (e)] and the corresponding SAED pattern [(b), (d) and (f)]—taken during the TEM analyses for the slowly cooled steel samples having 10, 30 and 100 ppm—of the ferrite grain boundaries. Arrows and the white box in the images indicate grain boundaries and the areas from where the SAED patterns have been taken

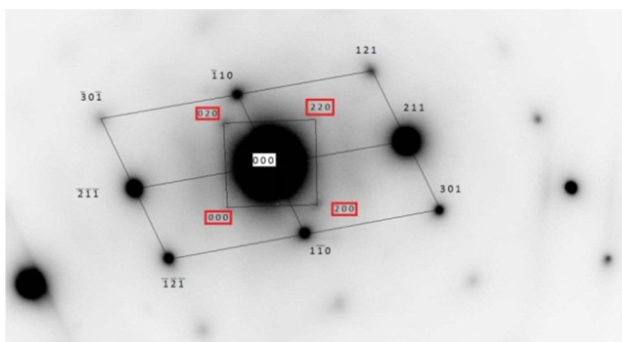


Fig. 11 A typical indexed SAED pattern of a precipitate found on the ferrite grain boundary confirming the precipitate to be BN. Red boxes indicate spots originating from the precipitate

culated for this steel chemistry (Ref 36-38). Also the majority of transformation is completed within 0.3 s (between 897 K (624 °C) and 873 K (600 °C); considering 75 K/s cooling rate). All these findings lead to the fact

that the transformation is displacive one in the steels with 30 and 70 ppm boron (Ref 36, 37).

3. For the steel with 10 and 100 ppm boron, the austenite to ferrite transformation completes well above 923 K (650 °C) where diffusion-controlled transformations are favored.

Hence, combining these observations one can expect that with 10 and 100 ppm boron steels would have microstructure comprising only of soft polygonal ferrite. On the contrary, for steels having 30 and 70 ppm boron, apart from softer polygonal ferrite, harder acicular and Widmanstatten ferrite can also be expected as a result of displacive transformation of austenite. Eventually, the hardness of the steel samples would increase as boron content increase from 10 to 70 ppm and thereafter decrease.

It has been seen (Fig. 9) for rapidly cooled (cooling rate greater than 10 K/s) steels that with the increasing boron content from 10 to 70 ppm, the amount of polygonal ferrite decreases. Also the irregularities in the ferrite boundary increase by forming quasi-polygonal ferrite and most impor-

tantly, acicularity in the microstructure increases appreciably (showing the presence of acicular and Widmanstätten ferrite). The hardness values measured on these samples also corroborate with the microstructural findings, i.e., the increase in phases of acicular morphology in the microstructure increases the hardness. However, for the sample having 100 ppm boron, acicularity in the microstructure is substantially low and fraction of polygonal/quasi-polygonal ferrite is substantially high (Fig. 9). This sample also shows minimum hardness for different cooling rates (Fig. 8a). Hence, it is rational to infer that boron in the range of 10–70 ppm in low carbon steel gives rise to increased hardness by favoring the formation of acicular microstructure even under a moderate cooling rate of 10 K/s. The presence of polygonal/quasi-polygonal ferrite—which causes lower hardness—was observed in the microstructure for the steel sample containing 100 ppm boron. This observation matches well with the microstructural prediction made from the dilation curves.

Transmission electron microscopic studies reveal that the boron content increases the amount of BN precipitate in steels. Boron is an effective nitride former, and the precipitation temperature of BN is in the range of 1423 K (1150 °C), nearly 100 K higher than that of aluminum nitride (AlN) (Ref 39, 40). These precipitates are formed at much higher temperature than the T_s . Once these precipitates decorate the prior austenite grain boundaries, they act as nucleation sites for the polygonal ferrite. As the fraction of precipitates (and hence the ferrite nucleation sites) increases with boron content, it becomes easier for polygonal ferrite to nucleate and as a result, substantial increase (~ 70 K) in the transformation start temperature (T_s) for all cooling rates, because the increase in BN precipitation instead of atomic boron—it has been seen with the boron content—favored the nucleation of polygonal ferrite. However, the presence of acicular phases in the microstructure of steels having 30 and 70 ppm boron can only be explained by segregation of atomic boron to prior austenite grain boundaries that lead to suppression of the ferrite nucleation and eventually late decomposition temperatures, favoring the phases of displacive transformation.

Finally, it can be conjectured that there might be two competing phenomena while cooling the steel from austenite; first, segregation of atomic boron to prior austenite grain boundaries, thereby suppressing the formation of polygonal ferrite. Second, part of the boron added in the steel precipitates at the prior austenite grain boundaries in the form of BN instead of atomic boron which subsequently helps in nucleation of polygonal ferrite. With boron addition in range of 10–70 ppm, the first phenomenon was favored. However, with 100 ppm of boron in steel, availability of excess boron paved way for easy precipitation of BN precipitates and thus supersedes the phenomenon of atomic boron segregation.

5. Conclusions

The present investigation has led to the following conclusions:

1. Low carbon (0.04 wt.%) steel treated with boron content varied between 10 and 100 ppm is prepared in an open air laboratory induction furnace. No special treatment was given to steels to reduce the nitrogen content. The

boron-to-nitrogen ratio varied between 0.33 and 2.17. The manganese and silicon content of these steels were restricted below 0.1 wt.%. This strict control over steel chemistry ensures all the physico-mechanical properties of steel are governed by either soluble boron or boron nitride precipitate.

2. Tensile properties—A maxima in UTS have been found for steel containing 70 ppm B followed by a drop in 100 ppm B steel. As the size and morphology of ferrite grains of the as-forged steels were found to be independent of boron content. It is conjectured that the coarsening of dislocation cell structure under the influence of boron might be the reason for softening behavior. Ductility for all four steels was in the range of 30–40% without showing any dependence on the boron concentration.
3. Fracture surface of the tensile test specimens was found to contain increasing amount of equiaxial dimples with increasing boron content. This observation has led to conclude that the presence of boron nitride precipitates might act as a nucleation and accumulation site for micro-voids in the steel under static loading condition.
4. As excess boron traps free nitrogen and carbon; the yield point elongation and strain aging index were found to decrease monotonically and substantially with the boron-to-nitrogen ratio.
5. Nanoprecipitates of cubic BN—as observed under TEM—were evident at the ferrite grain boundaries. These precipitates played as nucleation sites for the polygonal ferrite at high temperatures.
6. Study on continuous cooling transformation behavior of boron-treated steels led to the fact that temperatures corresponding to austenite to ferrite transformation start (T_s) increase noticeably as boron content in the steel increases from 10 to 100 ppm. This might be due to availability of more number of BN precipitates which act as nucleation sites for ferrite at high temperatures and thus increase the austenite to ferrite transformation start temperature.
7. Microstructural observations of rapidly cooled (50 and 75 K/s) samples indicated that the formations of polygonal and quasi-polygonal ferrites become more favored compared to acicular ferrite as the boron content increases from 70 to 100 ppm, due to increase in preferential sites for the nucleation of these high-temperature phases that are provided by BN precipitates. Data on hardness measurements on the same samples confirm the fact by showing a maxima and a minima for the steels containing 70 and 100 ppm boron, respectively.
8. Based on all the experimental evidences of present investigation, it is conjectured that BN may play the role of nucleating agent for polygonal ferrite during transformation of austenite under continuous cooling condition (even at 75 K/s) and thus softening the steel.

Acknowledgments

The authors are thankful to the management of Tata Steel for providing the essential research facilities and permitting to publish this paper. Important technical inputs regarding strain aging index measurement was provided by Dr. Sourabh Chatterjee (R&D Tata Steel); authors take this opportunity to acknowledge his support. Authors also thank Dr. Mainak Ghosh of National Metallurgical

Laboratory, Jamshedpur, for his advice during sample preparation for TEM study and interpretations of images and SAED patterns.

References

1. G.F. Melloy, P.R. Slimmon, and P.P. Podgursky, Optimizing the Boron Effect, *Metall. Trans.*, 1973, **4**, p 2279–2289
2. M. Marucci, A. Lawley, R. Causton, and S. Saritas, Effect of Small Additions of Boron on the Mechanical Properties and Hardenability of Sintered P/M Steels. <http://www.hoeganaes.com/TechPapersv2/113.pdf>
3. H.R. Lin and G.H. Cheng, Hardenability Effect of Boron on Carbon Steels, *Mater. Sci. Technol.*, 1987, **3**(10), p 855–859
4. D.A. Mortimer and M.G. Nicholas, Surface and Grain-Boundary Energies of AISI 316 Stainless Steel in the Presence of Boron, *Met. Sci. J.*, 1976, **10**(9), p 326–332
5. J.C. Fisher, Influence of Boron on Hardenability of Steel, *J. Min. Met. & Mat. Soc.*, 1954, **6**(10), p 1146–1147
6. X.L. He, Grain Boundary Segregation of Boron, *Acta Metall*, 1989, **37**, p 147–161
7. K. Seto, D. Larson, P. Warren, and G.D. Smith, Grain Boundary Segregation in Boron Added Interstitial Free Steels Studied by 3-Dimensional Atom Probe, *Scr. Mater.*, 1999, **40**, p 1029–1034
8. D.A.P. Easterling and K.E. Easterling, *Phase Transformations in Metals and Alloys*, Van Nostrand Reinhold, Wokingham, 1981, p 272–273
9. O.M. Akselsen, O. Grong, and P.E.K.A. Comparative, Study of the Heat Affected Zone (HAZ) Properties of Boron Containing Low Carbon Steels, *Metall. Trans. A*, 1986, **17A**, p 1529–1536
10. K.A.T. Hansen and S.S. The, Boron Hardenability Effect in Thermo-mechanically Processed, Direct-Quenched 0.2 Pct C Steels, *Metall. Trans. A*, 1990, **21A**, p 1697
11. D.T. Llewellyn and W.T. Cook, Metallurgy of Boron-Treated Low-Alloy Steels, *Met. Technol.*, 1974, **1**(1), p 517–529
12. B.M. Kapadia, Effect of Boron Additions on Toughness of Heat-Treated Low Carbon Steel, *Hardenability Concepts with Applications to Steel*, C.V. Doane, J.S. Kirkaldy, Ed., AIME-TMS, Warrendale, 1978, p 448–482
13. C.R. Simcoe, A.R. Elsea, and G.K. Manning, Study of the Effect of Boron on the Decomposition of Austenite, *Trans. Met. Soc. AIME*, 1955, **7**(1), p 193–200
14. R.A. Grange and T.M. Garvey, Factors Affecting the Hardenability of Boron-Treated Steels, *Trans. ASM*, 1946, **37**, p 136–191
15. Y. Ohmori and K. Yamanaka, Hardenability of Boron-Treated Low Carbon Low Alloy Steel, *Boron in Steel*, S.K. Banerji, J.E. Moral, Ed., The Metallurgical Society of AIME, Warrendale, 1980, p 44–60
16. Ph. Maitrepierre, J. Rofes-Vernis, and D. Thievellier, Structure-Properties Relationships in Boron Steels, *Boron in Steel*, S.K. Banerji, J.E. Moral, Ed., The Metallurgical Society of AIME, Warrendale, 1980, p 1–18
17. J.B. Gilmour, G.R. Purdy, and J.S. Kirkaldy, Thermodynamics Controlling the Proeutectoid Ferrite Transformations in Fe-C-Mn Alloys, *Met. Trans.*, 1972, **3**(6), p 1455–1464
18. Ph. Maitrepierre, D. Thievellier, and R. Tricot, Influence of Boron on the Decomposition of Austenite in Low Carbon Alloyed Steels, *Metall. Trans. A*, 1975, **6**, p 287–301
19. V.V. Parusov, A.B. Sychkov, M.A. Zhigarev, and A.V. Perchatkin, *Wire Rod of Boron-Bearing Low-Carbon Steel for Direct Deep Drawing*, 2004, **48**, p 68–73
20. B. Yalamanchili, J. Nelson, P. Power, and D. Lanham, North Star Steel Texas: Experience with Boron Additions to Low-Carbon Steel, *Wire J. Int.*, 2001, **11**, p 90–94
21. A.R. Frank and A. Kirkcaldy, The Effect of Boron on the Properties of Electric-Arc-Sourced Plain Carbon Wire—Drawing Qualities, *Wire J. Int.*, 1998, **31**(5), p 100–113
22. A. Deva, B.K. Jha, and N.S. Mishra, Influence of Boron on Strain Hardening Behaviour and Ductility of Low Carbon Hot Rolled Steel, *Mater. Sci. Eng. A*, 2011, **528**, p 7375–7380
23. Y.R. Cho, S.I. Kim, and B.S. Seong, Effect of Boron Addition on the Microstructure and Mechanical Properties of Low-Carbon Steels, *Iron Steel Technol.*, 2004, **1**, p 46–51
24. C. Camurri, C. Carrasco, I. Bello, and M. Trucco, Development of Low Carbon Boron Steel for Wire Drawing, *Mater. Sci. Forum*, 2007, **539–543**, p 4238–4242
25. C. Camurri, C. Carrasco, I. Bello, and M. Trucco, Development of Low Carbon Boron Steel for Wire Drawing, *Mater. Sci. Forum*, 2007, **539–543**, p 4238–4242
26. B.B. Hundy, Accelerated Strain Ageing of Mild Steel, *J. Iron Steel Inst.*, 1954, **178**, p 34–38
27. J.R. Low and M. Gensamer, Aging and the Yield Point in Steel, *Trans. A.I.M.E.*, 1944, **158**, p 207–249
28. A.H. Cottrell and B.A. Bilby, Dislocation Theory of Yielding and Strain Ageing of Iron, *Proc. Phys. Soc.*, 1949, **62A**, p 49
29. J.D. Baird, Strain Aging of Steel—a Critical Review, *Iron Steel*, 1963, **36**, p 186–192
30. D.V. Wilson and B. Russell, The Contribution of Atmosphere Locking to the Strain-Ageing of Low Carbon Steels, *Acta Metall.*, 1960, **8**, p 36–45
31. H.R. Lin and G.H. Cheng, Analysis of Hardenability Effect of Boron, *Mater. Sci. Technol.*, 1990, **6**(8), p 724–730
32. S. Khare, Approximations in Using Solubility Products for B, N, Ti and Al, *Mater. Sci. Technol.*, 2011, **27**, p 1863–1868
33. S.W.T. George Krauss, Ferritic Microstructures in Continuously Cooled Low- and Ultralow-Carbon Steels, *ISIJ Int.*, 1995, **35**, p 937–945
34. W.C. Jeong, Microstructural Aspects of Quasi-Polygonal and Granular Bainitic Ferrites in an Ultra-Low-Carbon Interstitial-Free High-Strength Steel, *Metall. Mater. Trans.*, 2003, **34A**, p 2025–2026
35. H.J. Jun, J.S. Kang, D.H. Seo, K.B. Kang, and C.G. Park, Effects of Deformation and Boron on Microstructure and Continuous Cooling Transformation in Low Carbon HSLA Steels, *Mater. Sci. Eng. A*, 2006, **422**(1-2), p 157–162
36. H.K.D.H. Bhadeshia, A Thermodynamic Analysis of Isothermal Transformation Diagrams, *Met. Sci.*, 1982, **16**, p 159–165
37. H.K.D.H. Bhadeshia, *Bainite in Steels*, Institute of Materials, London, 2001, p 1–450
38. H.K.D.H. Bhadeshia, Rationalisation of Shear Transformations in Steels, *Acta Metall.*, 1981, **29**, p 1117–1130
39. S. Khare, Approximations in Using Solubility Products for B, N, Ti and Al, *Mater. Sci. Technol.*, 2011, **27**, p 1863–1868
40. M.S. Yaghmaee, Equilibria in the Liquid Quaternary Fe-Al-N-B System (2000). <http://www.uni-miskolc.hu/~fkmsahba/Publication-view/2001/2001-F4.pdf>